EARTH & PLANETARY SCIENCE LETTERS

ELSEVIER

Contents lists available at SciVerse ScienceDirect

Earth and Planetary Science Letters

Letters

Laboratory simulations of tensile fracture development in a volcanic conduit via cyclic magma pressurisation

Philip M. Benson [a,b,*], Michael J. Heap [c], Yan Lavallée [d], Asher Flaws [d], K.-U. Hess [d], A.P.S. Selvadurai [e], Donald B. Dingwell [d], B. Schillinger [f]

[a] Geological Institute, Department of Earth Sciences, Swiss Federal Institute of Technology, Zurich 8092, Switzerland
[b] Rock Mechanics Laboratory, School of Earth and Environment, University of Portsmouth, Portsmouth PO1 3QL, UK
[c] Ecole et Observatoire des Sciences de la Terre, Université de Strasbourg (UMR 7516 Centre National de la Recherche Scientifique), France
[d] Earth and Environment, LMU—University of Munich, Theresienstr. 41, 80333 München, Germany
[e] Department of Civil Engineering and Applied Mechanics, McGill University, Montreal, Quebec, Canada H3A 2K6
[f] Forschungsreaktor FRM-II, Technische Universität München, 85747 Garching, Germany

ARTICLE INFO

ABSTRACT

During volcanic unrest, high magma pressure induces cracking and faulting of the country rock, providing conduits for the transport of magma and other fluids. These conduits, known as dykes, are fundamental structures for the transport of magma to the surface in volcanically active regions. The mechanics of dyke propagation is not yet fully understood but is crucial to better model dyke emplacement and eruption in volcanoes. Central to this need is a greater understanding of the mechanical properties of the magma/country rock interaction as a function of known magmatic pressure, temperature and stress. Here, we report data from a series of experiments in which we cyclically compress viscoelastic rhyolitic magma (at 828 °C, 892 °C and 918 °C) inside a cylindrical conduit-like shell of basalt (from Mt. Etna, Italy) until fracture occurs. The compression is performed under strain rates cyclically varying between 5×10^{-6} and $5 \times 10^{-5}\,\mathrm{s}^{-1}$. The resultant monitored (axial) loading and relaxation illustrates how the presence of a visco-elastic fluid (magma) controls the stress induced at the conduit margin boundary. This is achieved by analysing the viscoelastic relaxation (through time) to calculate an apparent modulus, which is found to decrease with both increasing temperature and time. In the 4 cycles before failure we find that the apparent modulus decreases from 180 to 40 GPa, 80 to 20 GPa and 8 to 1 GPa for imposed stress cycles at 828 °C, 892 °C and 918 °C, respectively. We theoretically estimate a tensile strength at failure of approximately 7–11 MPa, consistent with recent field data and in agreement with a model derived from the sample geometry and basic material parameters. Post-experimental neutron computed tomography and microscopic analyses further reveal the fragmentation of the melt and generation of tuffisite veins inside the conduit due to spontaneous crack nucleation associated with conduit wall fracture. The geometry of the rupture area inside the melt is akin to a Mach cone associated with supershear fractures. We discuss our findings in terms of magma-rock interaction leading to dykes, tuffisite veins and magma fragmentation.

1. Introduction

The link between magmatism and tectonic structures has long been recognised (e.g. Nakamura, 1977; De Natale et al., 1997; Acocella et al., 2001; Lavallée et al., 2009; Gundmundsson, 2011a). For instance, pressure gradients force magma to ascend through the crust via the process of tensile failure in the country rock at the propagating dyke tip, aided by any existing faults and fractures (Pitcher, 1979). Movement into and through these pathways produces stress fluctuations that act against the host rock and the local/regional tectonic stress field (Hutton, 1996). If the local strength of the rock is exceeded, the resultant failure will modify the stress field (Pertsov et al., 1977; Bonafede and Danesi, 2010), with repercussions on the chemical equilibrium of the magma under the new pressure conditions as well as creating new pathways to divert its course of ascent and to transport exsolved gases. Therefore, dyking exerts a primary control on the integrity of the host rocks whilst simultaneously affecting the physical and chemical evolution of the magma as it attempts to

reach the surface and erupt. It follows that our assessments of volcanic hazards fundamentally rely on our knowledge of host rock failure, dyke injection and magma transport—processes controlled by the mechanical properties of the rock and the rheological behaviour of the intruding magma (e.g. Gundmundsson, 2011a).

The failure of rocks is initiated largely in tension (Griffith, 1920), owing to the tensile strength of rocks being approximately a tenth of their compressive strength (Jaeger et al., 2007). Shear faulting is essentially a result of the linkage of many smaller tensile cracks (e.g. Paterson and Wong, 2005). Once nucleated, fractures can further propagate due to perturbation of the elastic energy release rate or the stress intensity factor at the crack tips (Inglis, 1913; Broek, 1982). In the case of dyke propagation at high temperatures, the viscoelastic response of the rock, creep (sub-critical crack growth) at the dyke tips may accelerate the propagation by one order of magnitude (Chen and Jin, 2011). Experimental studies have mapped out the fracture toughness of volcanic rocks subjected to a range of temperatures and confining pressures (Rocchi et al., 2004; Balme et al., 2004; Smith et al., 2009). These findings therefore suggest that the propagation of tensile fractures would ease as they extend towards the Earth's surface, a scenario usually favoured in numerical simulations (e.g. Santoni et al., 2011). Although this result can be explained by reference to the classical Griffith energy balance scenario it is important to also acknowledge that, on the other hand, disconti-nuities are more likely to be open near to the surface leading to the Cook–Gordon analysis of crack arrest (Gudmundsson, 2009). In the volcanic context, magma can more easily infiltrate tensile fractures as seen in sheet-like dike structures with evidence of elastic wall deformation (e.g. Cuevas et al., 2006). Field and theoretical studies have, however, shown that the majority of dykes are arrested at depth (Gudmundsson and Brenner, 2001, 2004). In the Campi Flegrei caldera (Naples, Italy), for example, very few dykes are exposed at the surface due to the soft overburden (e.g. De Natale et al., 1997), creating stress-release barriers that adversely influence the ability of the dyke tip to propagate further (Gundmundsson, 2011a). The source of these discrepancies may partly reside in the stress imparted by the magma.

During ascent, the physical, chemical and thus rheological properties of magma evolve (Sparks et al., 1997). Changes in pressure and temperature force crystallisation and the exsolution of volatiles which promote an increase in viscosity (Hess and Dingwell, 1996; Lejeune and Richet, 1995) as well as an increase in pore pressure (Massol and Jaupart, 1999). These end effects counteract one another during the magma-driven fracture pro-pagation through the crust (Carrigan, 2000), an increase in viscosity serves to slow magma migration, whereas an increase in pore fluid pressure favours cracking of the host rock. In addition, bubble segregation from the magma followed by accu-mulation near the fracture tip can amplify the local stress to exceed the fracture toughness. The relationship between the magma rheology, the rock strength and the stress field generated at their interface is thus fundamental to our understanding of fracturing, dyking and magma transport.

Experimental investigations of fracturing, dyking and magma transport are scarce. Work has concentrated either on analogue setups using gelatine and other materials that are fractured by injection of coloured water (Menand and Tait, 2001; Acocella et al., 2001; Walter and Troll, 2003), or – for simulation of representative rock properties – a simplified experimental setup at room temperatures. In the latter case, hydrofracturing is caused by increasing the water pressure within an axial conduit (cored out of a cylindrical rock shell) flanked by a rubber membrane (to isolate the fluid from the rock) until failure of the rock shell (e.g. Vinciguerra et al., 2004). Although useful for visualising the physical processes occurring during dynamic fracturing, this type of experiment cannot reveal the interaction between the dyke tip and the host rock because the pressurising medium is mechani-cally coupled to the inner bore by the membrane. In addition, since this type of experiment is conducted at low temperatures, it cannot reproduce the behaviour of magma interacting with the host rock. Here, we experimentally simulate magma–rock interaction by compressing a magma inside a conduit-like cylind-rical shell until fracturing of the shell occurs. The experiments provide an estimate of the magma stress relaxation and the tensile strength of the conduit wall rocks at high temperatures, as well as a description of the physics occurring at the onset of dyking.

2. Methods

Magma–rock failure tests were performed by combining Cougar Creek obsidian, CO, (from the Cougar Creek lava flow, Yellowstone National Park, USA; see Christiansen, 2001), and Etna basalt, EB, (from Mt. Etna volcano, Italy) in an experimental setup analogous to hydraulic fracture experiments (see below for details). The selected obsidian is a dense (porosity of $< 0.1\%$), aphyric rhyolite, simulating flow of a single-phase silicate melt at high temperature. The basalt is a porphyritic, alkali basalt of approximately 3.8% porosity. It comprises millimetre-size pheno-crysts of pyroxene, olivine and feldspar within a fully crystallised, fine-grained groundmass. The basalt was chosen because it has been extensively studied (Stanchits et al., 2006; Benson et al., 2007, 2010; Heap et al., 2009, 2011) and because its properties are nearly isotropic (e.g. ultrasonic wave velocities) and tempera-ture independent (the mechanical strength was found to be independent of temperature up to 900 °C). Furthermore, this basalt contains no glass, so it should not undergo softening at the investigated temperatures. Thus, these materials were selected since the rhyolite can deform viscously while the basalt will remain brittle under the given experimental temperatures. Our study was carried out in three phases.
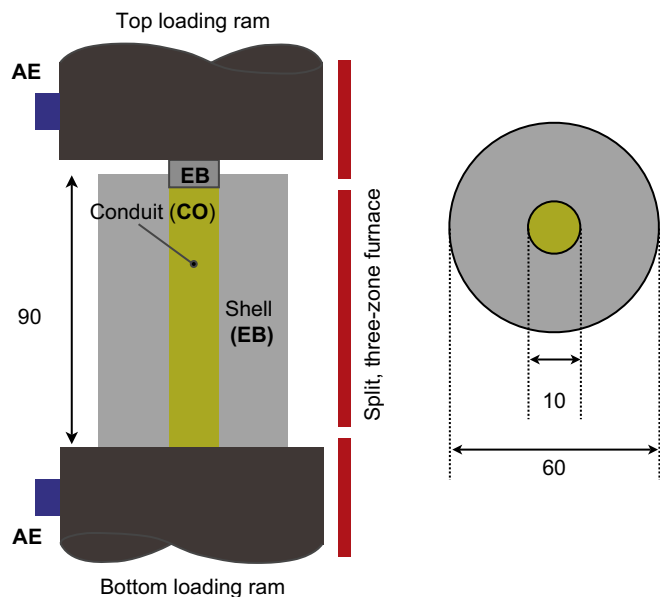
Firstly, we characterised the viscosity–temperature relationship of the rhyolitic melt to be used as a guide for our experimental temperatures. We employed the standard micropenetration tech-nique using a Baehr vertical dilatometer, which involved monitor-ing the penetration rate of an indenter (of known geometrical end shape) into a disc of melt (Hess and Dingwell, 1996). The rate of indentation of a small melt disc (6 mm in diameter and 3 mm in thickness) was used to compute the viscosity as a function of temperature, according to:

$$\eta_{shear} = \frac{0.1875Ft}{r^{0.5}\alpha^{1.5}} \tag{1}$$

where F is the force applied by the indenter, t the time of indentation, r the indenter radius, and α the indented depth. This method resolves the viscosity to within $+/-0.05$ log unit of viscosity (Hess and Dingwell, 1996).

Secondly, the uniaxial compressive strength of the basalt was investigated at a range of temperatures (25, 200, 500, 750, 900 and 950 °C) on cylindrical cores (25 mm in diameter and 75 mm in length) in a high-temperature uniaxial press (a full description of the uniaxial press can be found in Hess et al., 2007). The strength tests were performed under the same variable strain rates as used in the magma–rock failure tests (see below).

Finally, magma–rock failure tests were performed in the high-temperature uniaxial press by pressing a plug of basalt (a disc 10 mm in diameter and 10 mm in length) onto a central core of rhyolitic melt (10 mm in diameter and 85 mm in length) encased by an outer shell of basalt (60 mm in diameter and 90 mm in

Top loading ram

AE

EB

Conduit (CO)

90

Shell (EB)

Split, three-zone furnace

AE

Bottom loading ram

10

60

Fig. 1. Experimental setup in side view (left) and plan view (right). The composite sample of Cougar Creek Obsidian (CO) is encased by a shell of basalt (EB) and topped by a hard basaltic plug. Compression of the plug, and thus the rhyolitic melt, was achieved using a servo-controlled hydraulic apparatus, within a 3 zone split furnace (shown schematically by the red bars). Dimensions are in millimetres; note that the AE sensors are mounted some distance from the furnace to avoid damage.

length; Fig. 1). The plug of basalt ensured that the inner conduit could be loaded without the loss of melt. Pressurisation of the inner melt was achieved by cyclically changing the imposed axial strain rate between 3.2×10^{-5} s^{-1} for 30 s and 1.3×10^{-6} s^{-1} for 300 s, thus yielding an average of 6.5×10^{-6} s^{-1}. This cyclicity was applied in an attempt to best simulate the cyclic pressurisation inferred from volcanic conduits (Vinciguerra et al., 2005). Based on the magma viscosity determination and the rock mechanical tests, the experiments were performed at temperatures of 828 °C, 892 °C and 918 °C in order to observe the potential influence of the magma on the host rock. During the experiments, the force applied to the melt was transmitted as an internal fluid (magma) pressure (due to the incompressibility of the silicate melt) onto the conduit inner shell (e.g. Valko and Economides, 1995). Essentially, the magma pressure acts against the inner surface of the conduit inducing failure in a manner analogous to hydrofracturing in rock mechanics. Deformation and failure was additionally monitored by a pair of acoustic emission (AE) sensors mounted directly on the loading pistons, to record the microseismicity generated at the point of shell failure; this microseismicity was scaled to fracturing on the tectonic scale (Burlini et al., 2007; Benson et al., 2007, 2010). The experiments were halted after failure of the shell, as confirmed by an obvious peak in AE energy and a substantial (to near-zero value) axial stress drop. The samples were then subjected to structural analysis, and the mechanical data were used in a numerical computation.

Post-experimental structural analyses were performed on the sample using neutron computed tomography (NCT), carried out at the ANTARES detector and FRM II cold neutron beam facility installed at Garching, Germany (Muhlbauer et al., 2005). Reconstructed images from the NCT have a voxel size of approximately 40 μm, permitting a simplified 3-D reconstruction of the internal structure of the samples and the extensive fracture patterns produced by the tensile stresses. Moreover, examination of the fracture network was also performed using transmitted light and reflected fluorescent light microscopy.

3. Results and analysis

3.1. Conduit melt viscosity

The temperature dependence of viscosity investigated through micropenetration shows that the Cougar Creek rhyolitic melt is a strong melt (low fragility index), with a near Arrhenian behaviour (Fig. 2). The viscosity data shows a standard deviation below 0.05 log unit of viscosity. Application of the Vogel–Fulcher–Tammann (VFT) equation resolves the viscosity (η) to:

$$\log\eta = A + \frac{B}{T-C} \tag{2}$$

where T is the temperature in Celsius, valid between the investigated temperature range of 750 and 920 °C, and $A = -0.6505$, $B = 7342$, and $C = -132$.

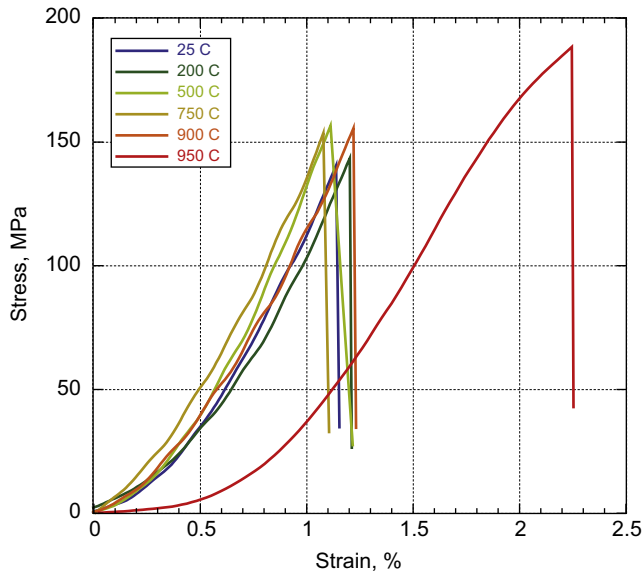### 3.2. Uniaxial compressive strength of the basalt

The uniaxial compressive strength of the basalt was investigated at a range of temperatures (25, 200, 500, 750, 900 and 950 °C) in order to probe potential changes in the mechanical behaviour. Brittle failure was observed in all samples (Fig. 3). Below 950 °C the strength remained approximately 150 MPa and did not vary systematically with temperature. At 950 °C the sample demonstrated mild changes in the mechanical behaviour, resulting in an increase in the peak stress and total strain at failure. Altogether, the data yielded values comparable to complementary studies (e.g., Heap et al., 2010).

3.3. Magma–rock failure test

The mechanical behaviour of conduit failure due to magma pressurisation was investigated at three temperatures. Fig. 4 shows the evolution of stress (axially generated on the cylindrical end of the inner melt core) with strain of the magma. During the experiment at 828 °C (Fig. 4A), the first detection of accumulated stress occurred at approximately 2570 s, with a subsequent stress
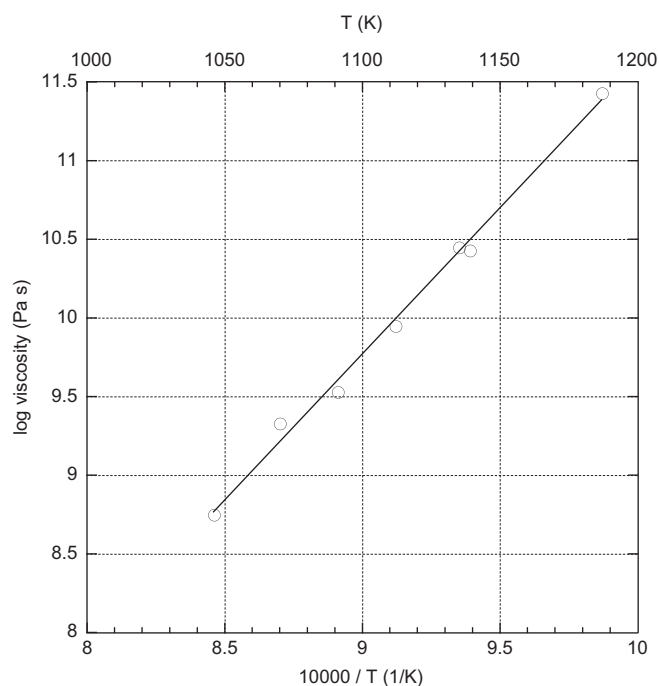
Fig. 2. Temperature dependence of the viscosity of Cougar Creek rhyolitic melt measured via the micropenetration technique in a Baehr vertical dilatometer.

Fig. 3. Uniaxial compressive strength (UCS) of the basalt as a function of temperature. The UCS is largely independent of temperature up to 900 °C.

drop noted as the strain rate entered its deceleration phase. The next cycle of strain rate acceleration/deceleration was also accompanied by a stress concentration/drop. The character of the third, fourth and fifth cycles of strain rate acceleration/deceleration were, however, significantly different in that a much higher stress accumulation was measured, of 25, 38 and 45 MPa respectively, and in each case an exponential stress drop occurred that did not fully recover to zero before the onset of the subsequent strain acceleration. The onset of pressure accumulation further coincided with the continuous release in acoustic emissions. The fifth and final cycle induced a stress drop to a low value (6–7 MPa) as a result of the complete failure of the outer shell. Failure was accompanied by a momentary increase in acoustic emissions. The two subsequent cycles of strain rate acceleration/deceleration showed that stress was incapable of accumulating and that acoustic emissions were fluctuating. The data show a clear dependence of the conduit pressure on the strain rate, since the peak stress increases in subsequent cycles, and the stress is released during the strain deceleration phases.

The general observations of stress concentration and relaxation as well as the accompanying acoustic emissions remain similar for all magma-conduit pressurisation tests, irrespective of the temperature. Temperature, which according to our investigation lowers the melt viscosity more than it affects the elastic behaviour of the shell (Fig. 2 vs. Fig. 3), speeds up relaxation during strain rate deceleration and delays failure of the shell (Fig. 4B and C). As the temperature increases the number of acceleration/deceleration cycles that lead to a lasting concentration of stress increases; once the stress accumulates, it is easier to maintain over time during the periods of slower strain rate (e.g. Fig. 4B 1050 s and 10500 s compared to Fig. 4C 10250 s and 10700 s).

4. Analysis

4.1. Structural analysis

Optical observation of the samples after the experiments clearly illustrates the tensile nature of the cracks that developed (Fig. 5). In plan view, the samples display two or three tensile cracks separated by angles of 180 or 120°, respectively, which
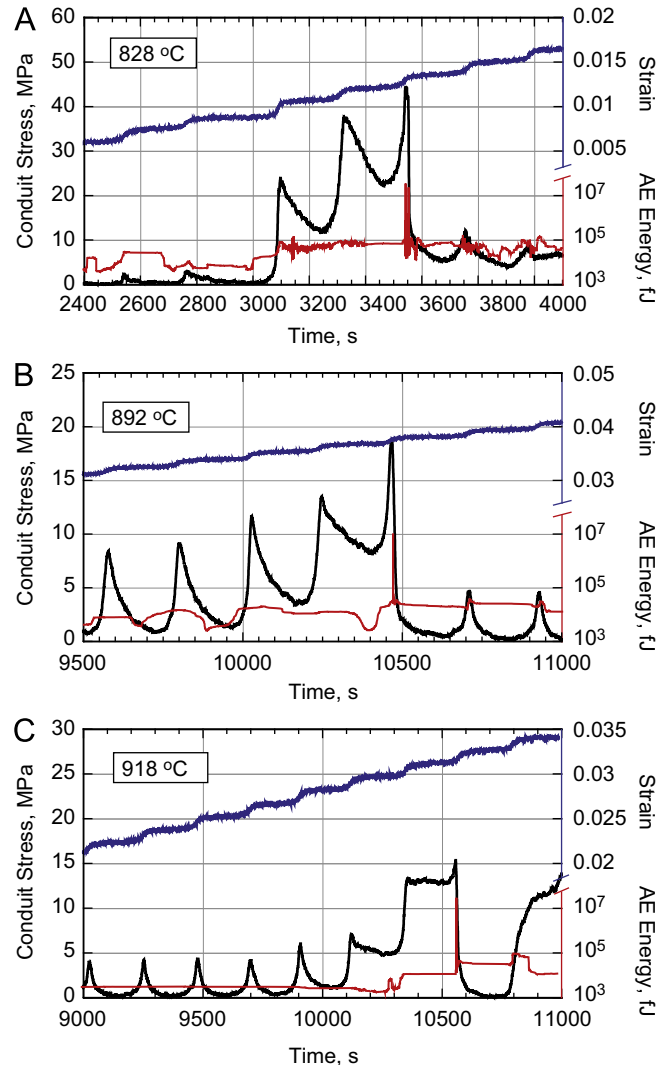

Fig. 4. Mechanical data during the cyclic magmatic conduit pressurisation. The data combines the conduit stressing/relaxation (black), the axial strain accumulated in the magma (blue), and the monitored AE (red) as a function of time, for experiments at (A) 828 °C, (B) 892 °C and (C) 918 °C. Cyclicity in strain rate acceleration/deceleration can be clearly seen as pressurisation of the conduit at high strain rate, which is then followed by relaxation during the period of low strain rates. A surge of AE is observed when the outer jacket experiences tensile failure at approximately (A) 3550 s, (B) 10475 s, and (C) 10560 s. (For interpretation of the references to colour in this figure legend, the reader is referred to the web version of this article.)

illustrate the axisymmetric nature of the setup. Axially, these cracks extend the entire length of each shell. The aperture of each fracture varies between each experiment; in some cases (Fig. 5, YE3), the sample fractured violently resulting in the presence of large glass fragments in the tensile cracks (Lavallée et al., 2012).

Post-test neutron computed tomography images of the sample revealed the continuity of each tensile fracture developed, from the outer to the inner margin of the shell (Fig. 6). An in-depth examination of the cracks clearly shows that they extend further into the rhyolite conduit. Microscopic analysis provides further details of the geometry of the cracks in the glass, which was a melt as it underwent brittle deformation. In detail, we observe a fragmented area hosting multiple micrometric cracks, converging towards the rupture tips, some 600 μm inside the glass (melt). The ability of a melt to fracture requires a strain rate faster than its relaxation rate. A complementary analysis of the criterion for failure of the melt during conduit fracturing is presented in
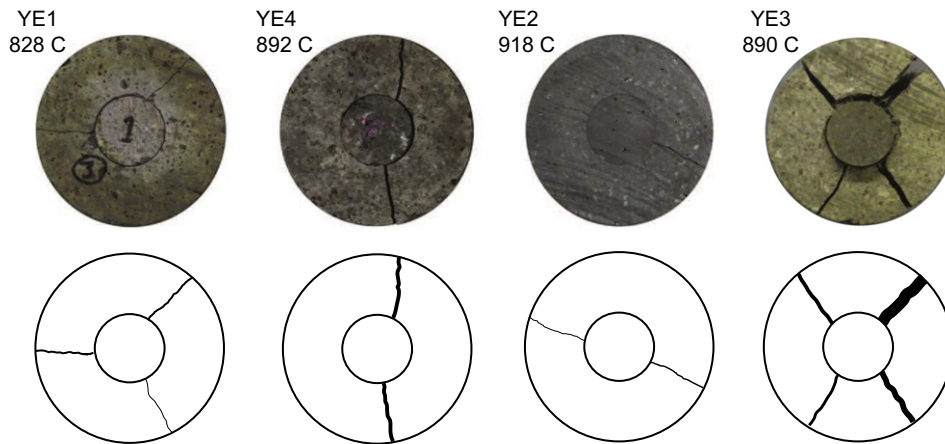
Fig. 5. Plan view images of the fractured outer shell, showing radial cracks in samples YE1 (828 °C), YE4 (892 °C), YE2 (918 °C) and YE3 (890 °C). The sketches below each image highlight the three (in the case of YE1), two (YE4 and YE2), or 4 (YE3) tensile cracks. At high strain rates, samples occasionally fracture in a violent manner (sample YE3, 890 °C), see text for details. Sample diameter is 60 mm.
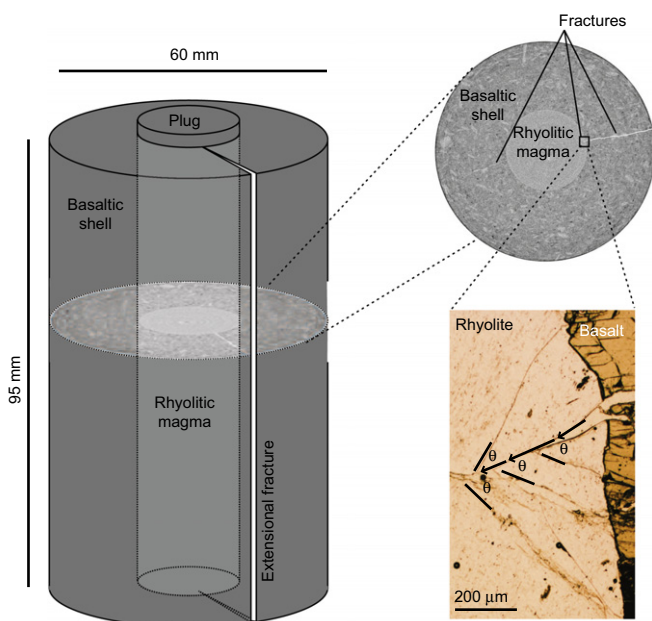
Fig. 6. Sketch of the fractures along with neutron computed tomographic images and transmitted light microphotograph of sample YE2 at 918 °C (modified from Lavallée et al., 2012). Neutron computed tomographic images reveal the continuous nature of the radial cracks along the conduit length. Detailed microscopic examination further highlights the fracturing of the inner core of rhyolitic melt. In transmitted light, we observed converging cracks and propagation direction (arrows) akin to a 'Mach cone' fossilised in the melt due to the catastrophic failure of the outer shell. Such 'shock cone' features generally form when fractures propagate faster than the local speed of sound, preserved in the (formerly molten) rhyolite at an angle θ to the fracture. Such features have been simulated in other studies (e.g. Xia et al., 2004).

Lavallée et al. (2012), suggesting that at the high strain rates inherent in these processes, even low-viscosity melts will deform in a brittle manner (e.g., Dingwell and Webb, 1989).

4.2. Visco-elastic relaxation

The stress-time data was analysed by considering (1) the relaxation of the stress during each period of strain rate deceleration, and (2) the peak stress at failure as a function of temperature (see *section iii* below). These respectively provided information on the rheological contribution of the melt and the mechanical contribution of the rock.

By examining the time-scale of stress release, it is possible to extract a quantitative relationship between the dynamic modulus of the melt in the conduit and the stress decay rate prior to shell failure. The analysis makes use of the known viscosity of the central rhyolitic melt at the temperatures of interest (Fig. 2), in order to derive an apparent modulus for the melt. Four cycles of strain-hold are considered prior to shell failure, and the Maxwell model adapted by Richter (2006) is used. This application is possible because the viscosity of a Newtonian melt remains constant at the tested strain rates:

$$\sigma(t) = \sigma_0 \exp\left[-\{t - t_L\}\frac{M_a}{\eta_t}\right] \qquad (3)$$

This analysis delivers the Young's modulus of the inner conduit (melt); however, for the purposes of our study, we adopt a generalised 'apparent' modulus (M_a). Other variables include time t, loading time t_L, peak stress σ_0, stress at time σ_t, and tensile viscosity η_t (Eq. (3)). Fig. 7 illustrates the first 100 s immediately after the commencement of the deceleration segments of the four cycles preceding shell failure (for each of the three experiments shown in Fig. 3). Application of Eq. (3) using measured viscosities of 8.3, 9.6 and 10 log unit (in Pa s), thus permits the calculation of the conduit stiffness with each cycle and temperature (Fig. 8). For all experiments, the stress decay exponent decreases (i.e. becomes flatter) moving from cycle 1 to 4. In terms of material stiffness, this result shows a decrease in modulus M_a from 180 to 30 MPa at 828 °C, from 80 MPa to 10 MPa at 892 °C and from 8 MPa to nearly zero MPa in the case of 918 °C. This suggests that the apparent modulus decreases as stress accumulates on the outer shell, leading to failure, as the temperature increases.

4.3. Peak stress at failure

The outer shell is most likely to fail when the hoop stress at its boundary exceeds the limiting tensile strength of the basalt. It is possible to estimate the tensile strength of the basalt shell using a combination of setup geometry and knowledge of the Young's modulus, the Poisson's ratio, and the material stiffness (as provided by Rocchi et al., 2004; Heap et al., 2011; Selvadurai and Benson, 2012). This analysis provides a direct measure of the stress accumulated in the magma at failure, and thus the resistance of magma to dyking.

In a recent study, Selvadurai and Benson (2012) theoretically examined the problem of the internal pressurisation of a hollow elastic cylinder of internal radius a and external radius b by a
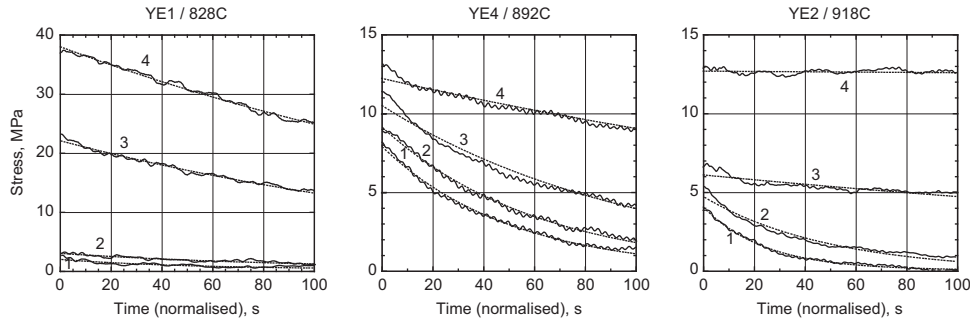
Fig. 7. Stress relaxation segments (first 100 s only) for the last 4 cycles (as shown in Fig. 4) prior to tensile failure of the confining basalt shell (Cycle 4 precedes failure).
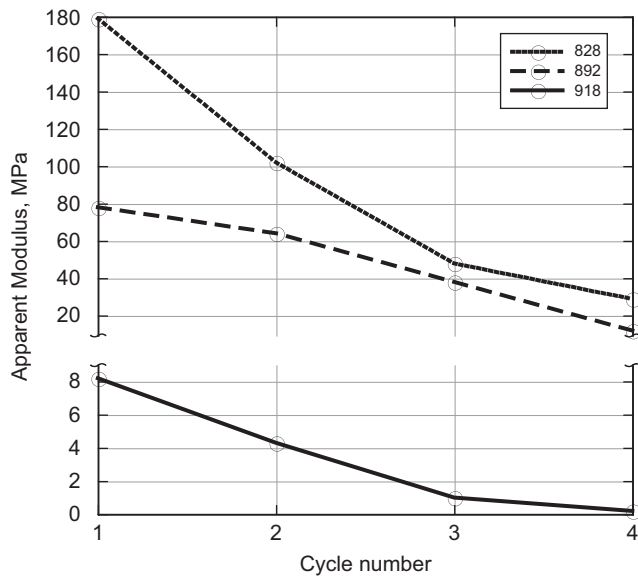

Fig. 8. Calculated apparent modulus (M) from viscoelastic relaxation parameters, using Eq. (3) (after Richter, 2006). The value of M is seen to decrease with both cycle number and increasing temperature.

smoothly embedded cylindrical elastic inclusion of identical length. The objective of their study was to use the smoothly embedded cylindrical elastic inclusion as a device for exerting a radial stress at the interface, which in turn would induce a tensile stress field in the hollow elastic cylinder. The use of an elastic cylindrical inclusion or plug to induce the hoop stress state in the annular cylinder is considered to be a more convenient and controllable loading configuration as opposed to the application of fluid pressures, which would entail abrupt rupture of the outer cylinder, particularly if the aspect ratio $(b/a)=\Gamma$ is marginally in excess of unity. The provision of a smooth interface between the cylindrical inclusion and the annular cylinder lends itself to the development of a relatively convenient closed form analytical solution based on the classical theory of elasticity. In an experiment, this interface has to be smooth to ensure the applicability of the theoretical results. [Note: the alternative to account for axial friction between the inner core and the external annular cylinder is much more difficult and the stress analysis of the resulting problem can only be performed through a computational approach (Selvadurai and Boulon, 1995).]

In the context of the application of the theoretical derivation to the present magma pressurisation problem, the outer annular cylinder can be regarded as the basaltic shell with isotropic Young's modulus E_R and Poisson's ratio v_R and the inner closely fitting elastic inclusion can be regarded as the conduit core of rhyolitic melt of isotropic Young's modulus E_C and Poisson's ratio

v_C. The inner core is subjected to a uniform axial compressive stress σ_A and the outer boundary of the annular basalt cylinder is maintained traction free. The analysis of the resulting elasticity problem is straightforward and the assumption of complete contact at the interface between the inner core and the external cylinder ensures that the radial displacement and the radial tractions exhibit continuity (Timoshenko and Goodier, 1970; Davis and Selvadurai, 1996; Selvadurai, 2000). The specifics of the analysis of the elastic plug compression problem are given in Selvadurai and Benson (2012), who also use the elastic inclusion compression approach to estimate the tensile strength of annular cylinders of Stanstead Granite. These studies also present an approach for estimating the Mode I fracture toughness of the geomaterial. The result of primary interest to the present paper relates to the tensile hoop stress that is generated at the boundary of the annular rock cylinder during compression of the central cylindrical elastic core by the axial compressive stress σ_A, which can be evaluated in exact closed form. For example, the tensile hoop stress at the inner boundary of the outer cylindrical rock can be evaluated using:

$$\sigma_{\theta\theta}^R(a) = |\sigma_A| \frac{v_C(\Gamma^2+1)}{(E_C/E_R[\Gamma^2(1+v_R)+(1-v_R)]+(1-v_C)(\Gamma^2-1))} \quad (4)$$

It is clear that in order for these stresses to develop, $v_C \neq 0$ and the analysis (Selvadurai and Benson, 2012) shows that the interface compressive stress is identical to the tensile hoop stress generated at the boundary of the rock. Of specific interest are the results applicable to the limiting case where the outer boundary of the core extends to infinity (i.e. $\Gamma \to \infty$). In this case the above results yield:

$$[\sigma_{\theta\theta}^R(a)]_{\Gamma\to\infty} = [\sigma^*]_{\Gamma\to\infty} = |\sigma_A| \frac{v_C}{(E_C(1+v_R)/E_R+(1-v_C))} \quad (5)$$

Known parameters in Eqs. (4) and (5) include the applied stress σ_A, the ratio of conduit to shell diameter Γ, the Poisson's ratios and Young's moduli for the outer shell and the core (v_C, E_C) and (v_R, E_R) respectively. The modulus of the conduit is calculated from the stress relaxation stage of the experiment discussed previously, leaving only the Poisson's ratio of the melt (0.35 ± 0.05) that is taken from previously published model data (Lister and Kerr, 1991). This permits the tensile stress to be calculated as a function of the applied stress. If this stress at the boundary of the country rock reaches the limiting tensile strength, fracture will occur.

To compare the theoretical fracture criteria with the laboratory data, Fig. 9 shows the theoretical (hoop) stress (given by Eq. (4)) as a function of the applied stress and a 'family' of representative Poisson's ratios (0.3–0.35–0.4) for the conduit, superimposed with the actual stress at which the samples failed (arrows). A clear relationship is seen whereby higher temperatures require a lower
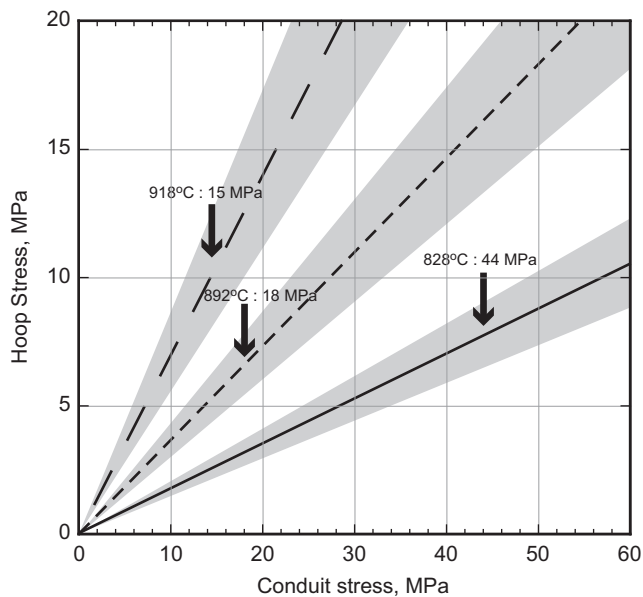
Fig. 9. Theoretical tensile failure strength as a function of internal magma pressure, inclusion modulus and temperatures. The magma pressurises until the shell fails in tension, denoted by arrows according to the maximum recorded conduit stress. Although the temperature of the experiments varies, a very similar hoop (tensile) stress at failure (i.e., 7–11 MPa) is calculated using Eq. (5).

conduit pressure in order to produce the same hoop stress, leading to fracture of the outer shell.

5. Discussion and conclusions

The dynamics of fracturing and associated magma movement through dykes is central to our understanding of mass transport and ultimately to our descriptions of volcanic eruptions (McNutt, 1996; Carracedo, 1999; Gudmundsson and Brenner, 2004; Collinson and Neuberg, 2011). Indeed, the accuracy of forecasting volcanic hazards posed by the propagation of dykes, as well as the stability/integrity of a volcanic conduit, strongly relies on probing the state of the host rocks at depth (e.g. Nakamura, 1977; Gudmundsson and Loetveit, 2005)—a task that cannot be achieved with current state of knowledge regarding monitored geophysical signals alone (McNutt, 1996; Smith et al., 2009). Models require the input of the path leading to various conduit fracture properties at depth and in volcanic edifices (e.g. Gudmundsson and Brenner, 2001; Vinciguerra et al., 2004). The present experimental and analytical investigation of magma–rock coupling to the problem of dyke initiation demonstrates the strong relationship between magma rheology and host rock elasticity. A decrease in the apparent Young's modulus of the magma precedes the tensile fracture of the host rock, which generates a local strain rate capable of fragmenting the magma.

Material stiffness is a key parameter of volcanic melts, and in many cases it is intimately linked to the explosivity of magma (e.g. Dingwell, 1996). The ability to estimate an apparent modulus of magma at depth would be helpful; since direct measurements are impractical, complimentary means must be employed to obtain such data. Our analysis suggests that it is possible to do so by incorporating measured viscous and elastic parameters (e.g. Table 1) in Eq. (4). For the case of the competent outer basalt shell, the Young's modulus and Poisson's ratio were measured directly and found to be essentially temperature invariant within our investigated temperature range (Heap et al., 2009), which is in broad agreement with the work of Rocchi et al. (2004).

Table 1

Sample/temperature (°C)	YE1/828	YE4/892	YE2/918
Poisson's ratio, v_{EB} (shell)	0.2	0.2	0.2
Poisson's ratio, v_{CO} (conduit)	0.3/0.35/0.4	0.3/0.35/0.4	0.3/0.35/0.4
Melt viscosity (log unit)	8.3	9.6	10.0
M_{EB} (MPa)	30	30	30

Likewise, the viscosity of the rhyolite melt is also known as a function of temperature. The least constrained parameter, the Poisson's ratio of the melt, was given a central value of 0.35 with a spread of 0.05 to calculate the tensile fracturing. The lower and centre estimates for Poisson's ratio within this range have been suggested in the small number of studies done to date (Gudmundsson, 1988; Rubin, 1995; Carpenter and Cash, 1988; Chu et al., 2010), with the upper end data measured at room temperature. Our analysis resolves the tensile (hoop) stress required to fracture the outer shell to be approximately 7 to 11 MPa, irrespective of the viscosity of the conduit. This agrees with field estimates for the tensile strength of rocks important in dyke propagation of approximately 6–9 MPa (Gudmundsson, 2011a, 2011b).

The stress relaxation is analysed using the Maxwell–Zener model (Richter, 2006). Specifically, our experiments suggest that a noticeable decrease in the apparent modulus M_a precedes failure. Although this is counterintuitive, such an effect could be produced if, as the cycles proceeded, an increase in shear stresses is present on the boundary of both the conduit and the inner shell surface. This is definitely a possibility since, in our experiment, pressurisation of the magma against the conduit wall is accompanied by an increased surface area of contact (i.e., initially, there is a narrow < 0.1 mm gap between the melt and the shell due to abrasion during sample preparation). Additionally, there may be rheological changes taking place due to melt pressurisation. Whether thixotropy of the melt comes into play in our investigation is rather unlikely since pressurisation of the low-viscosity melt was performed at strain rates far slower than the onset of non-Newtonain behaviour calculated via Maxwell relaxation time scale (e.g., Dingwell and Webb, 1989; see Lavallée et al., 2012). As to the likelihood that the visco-elastic behaviour of the melt is modified with increasing pressurisation, magmas are generally regarded as visco-elastic liquids with very restricted influence of pressure on the viscosity (Dingwell, 1998). It thus seems most likely that the observed apparent modulus decrease results from a combination of viscous relaxation and release of the elastic stress of the shell accumulated at the inner margin. The ability to probe for this apparent modulus in nature would thus offer a window for both the magma viscosity and the conduit wall elastic response.

Finally, it should be emphasised that the post-failure observations revealed fracturing of the melt inside the conduit. Rheological and acoustic analysis of the criterion for failure of the melt during conduit fracturing is presented in Lavallée et al. (2012), suggesting that at the high strain rates inherent in these processes, even low-viscosity melts will deform in a brittle manner (e.g., Dingwell and Webb, 1989). A close analysis of the fracture tip and surrounding crack geometry reveals a remarkable similarity to a Mach cone. Such 'shock cone' features generally form in spontaneously nucleated supershear ruptures, propagating faster than the local speed of sound (e.g. Xia et al., 2004), fossilised here in the (formerly molten) rhyolite at an angle θ to the fracture. Whether the cone formed as a result of sub-Rayleigh tensional cracking of the melt during conduit shell failure or due to spontaneous supershear rupture cannot be ascertained through

our post-experiment analysis; it nonetheless remains evident that magma can fragment during wall rock failure. This observation alone is important to our understanding of dyke nucleation and propagation, because not only does magma failure instigate the generation of tuffisite veins (Lavallée et al., 2012), it also contributes to the seismic record (Lavallée et al., 2008; Tuffen et al., 2003, 2008), masking the precursor signal for dyke propagation and, potentially, explosive eruptions.

In summary, the combined experimental (mechanical and AE) and analytical simulations of conduit failure induced by the inner compression of magma show that:

(a) The coupling of stress, strain and seismic data through time can be used to infer the stability of volcanic conduits and/or the state of the magma during periods of unrest via the calculation of viscoelastic relaxation parameters and hence the modulus (or viscosity) of the melt.
(b) Dyke nucleation initiates when the tensile strength of the host rocks is overcome by the magmatic pressure. In the case of the investigated basalt from Mt. Etna, the calculated tensile strength is temperature invariant and approximates 7–11 MPa.
(c) Conduit wall rock failure generates an energetic strain wave, with some evidence of this being a supershear feature, capable of locally fragmenting magma, thereby promoting the production of tuffisite veins and, potentially, episodes of explosive activity.

Acknowledgements

References

Acocella, V., Cifelli, F., Funiciello, R., 2001. The control of overburden thickness on resurgent domes: insights from analogue models. J. Volcanol. Geotherm. Res. 111, 137–153.
Balme, M.R., Rocchi, V., Jones, C., Sammonds, P.R., Meredith, P.G., Boon, S., 2004. Fracture toughness measurements on igneous rocks using a high-pressure, high-temperature rock fracture mechanics cell. J. Volcanol. Geotherm. Res. 132 (2–3), 159–172.
Benson, P.M., Thompson, B.D., Meredith, P.G., Vinciguerra, S., Young, R.P., 2007. Imaging slow failure in triaxially deformed Etna basalt using 3D acoustic-emission location and X-ray computed tomography. Geophys. Res. Lett. 34 (1–5), L03303, http://dx.doi.org/10.1029/2006GL028721.
Benson, P.M., Vinciguerra, S., Meredith, P.G., Young, R.P., 2010. Spatio-temporal evolution of volcano seismicity: a laboratory study. Earth Planet. Sci. Lett. 297, 315–323.
Bonafede, M., Danesi, S., 2010. Near-field modifications of stress induced by dyke injection at shallow depth. Geophys. J. Int. 130, 435–448, , http://dx.doi.org/10.1111/j.1365-246X.1997.tb05659.x.
Broek, D., 1982. Elementary Engineering Fracture Mechanics. Martins Nijhoft Publishers, The Hague, Netherlands.
Burlini, L., Vinciguerra, S., Di Toro, G., De Natale, G., Meredith, P.G., Burg, J.-P., 2007. Seismicity preceding volcanic eruptions: new experimental insights. Geology 35, 183–186.
Carracedo, J.C., 1999. Growth, structure, instability and collapse of Canarian volcanoes and comparisons with Hawaiian volcanoes. J. Volcanol. Geotherm. Res. 94, 1–19.
Carrigan, C.R., 2000. Plumbing systems. In: Sigurdson, H. (Ed.), Encyclopedia of Volcanoes. Academic Press, London, pp. 219–235.
Carpenter, P.J., Cash, D.J., 1988. Poisson's ratio in the valles caldera and Rio Grande rift of Nothern New Mexico. BSSA 78 (5), 1826–1829.
Chen, Z., Jin, Z.-H., 2011. Subcritical dyke propagation in a host rock with temperature-dependent viscoelastic properties. Geophys. J. Int. 186 (3), 1095–1103, http://dx.doi.org/10.1111/j.1365-246X.2011.05113.x.
Christiansen, R.L., 2001. The Quaternary and Pliocene Yellowstone plateau Volcanic Field of Wyoming, Idaho and Montana. U.S. Department of the Interior, U.S. Geological Survey. Professional Paper 729-G, U.S. Geological Survey, Reston, Virginia.
Chu, R., Helmberger, D.V., Sun, D., Jackson, J.M., Zhu, L., 2010. Mushy magma beneath Yellowstone. Geophys. Res. Lett. 37 (1–5), L01306, http://dx.doi.org/10.1029/2009GL041656.
Collinson, A.S.D., Neuberg, J.W., 2012. Gas storage, transport and pressure changes in an evolving permeable volcanic edifice. J. Volcanol. Geotherm. Res., 243–244, 1–13, ⟨http://dx.doi.org/10.1016/j.jvolgeores.2012.06.027⟩.
Cuevas, J., Esteban, J.J., Tubia, J.M., 2006. Tectonic implications of the granite dyke swarm in the Ronda peridotites (Betic Cordilleras, Southern Spain). J. Geol. Soc. 163, 631–640, , http://dx.doi.org/10.1144/0016-764905-038.
Davis, R.O., Selvadurai, A.P.S., 1996. Elasticity and Geomechanics. Cambridge University Press, Cambridge.
De Natale, G., Petrazzuoli, S.M., Pingue, F., 1997. The effect of collapse structures on ground deformations in calderas. Geophys. Res. Lett. 24 (13), 1555–1558.
Dingwell, D.B., Webb, S.L., 1989. Structural relaxation in silicate melts and non-Newtonian melt rheology in geologic processes. Phys. Chem. Miner. 16 (5), 508–516.
Dingwell, D.B., 1996. Volcanic dilemma: flow or blow? Science 273 (5278), 1054–1055.
Dingwell, D.B., 1998. Melt viscosity and diffusion under elevated pressures. Rev. Mineral. Geochem. 37, 397–424.
Griffith, A., 1920. The phenomena of rupture and flow in solids. Philos. Trans. R. Soc. London, Series A 221, 163–198.
Gudmundsson, A., 1988. Effect of tensile stress concentration around magma chambers on intrusion and extrusion frequencies. J. Volcanol. Geotherm. Res. 35, 179–194.
Gudmundsson, A., 2009. Toughness and failure of volcanic edifices. Tectonophysics 471 (1–2), 27–35.
Gundmundsson, A., 2011a. Deflection of dykes into sills at discontinuities and magma-chamber formation. Tectonophysics 500, 50–64.
Gudmundsson, A., 2011b. Rock Fractures in Geological Processes. CUP (pp. 592).
Gudmundsson, A., Brenner, S.L., 2001. How hydrofractures become arrested. Terra Nova 13 (6), 456–462.
Gudmundsson, A., Brenner, S.L., 2004. Local stresses, dyke arrest and surface deformation in volcanic edifices and rift zones. Ann. Geophys. 47 (4), 1433–1454.
Gudmundsson, A., Loetveit, I.F., 2005. Dyke emplacement in a layered and faulted rift zone. J. Volcanol. Geotherm. Res. 144, 311–327.
Heap, M.J., Vinciguerra, S., Meredith, P.G., 2009. The evolution of elastic moduli with increasing crack damage during cyclic stressing of a basalt from Mt. Etna volcano. Tectonophysics 471, 153–160.
Heap, M.J., Faulkner, D.R., Meredith, P.G., Vinciguerra, S., 2010. Elastic moduli evolution and accompanying stress changes with increasing crack damage during the cyclic stressing of rocks. Geophys. J. Int. 183, 225–236.
Heap, M.J., Baud, P., Meredith, P.G., Vinciguerra, S., Bell, A.F., Main, I.G., 2011. Brittle creep in basalt: implications for time-dependent volcano deformation. Earth Planet. Sci. Lett. 307, 71–82.
Hess, K.U., Dingwell, D.B., 1996. Viscosities of hydrous leucogranitic melts: a non-Arrhenian model. Am. Mineral. 81, 1297–1300.
Hess, K.U., Cordonnier, B., Lavallée, Y., Dingwell, D.B., 2007. High-load, high-temperature deformation apparatus for synthetic and natural silicate melts. Rev. Sci. Instrum. 78 (7), 1–4, 075102.
Hutton, D.H.W., 1996. The 'space problem' in the emplacement of granite. Episodes 19, 114–119.
Inglis, C.E., 1913. Stresses in a plate due to the presence of cracks and sharp corners. Trans. Inst. Nav. Archit. 55, 219–241.
Jaeger, J., Cook, N.G.W., Zimmerman, R., 2007. Fundamentals in Rock Mechanics, fourth ed. Blackwell Publishing, London (pp. 475).
Lavallée, Y., Meredith, P.G., Dingwell, D.B., Hess, K.U., Wassermann, J., Cordonnier, B., Gerik, A., Kruhl, J.H., 2008. Seismogenic lavas and explosive eruption forecasting. Nature 453, 507–510.
Lavallée, Y., de Silva, S., Salas, G., Byrnes, J.M., 2009. Structural control of a rotated graben on volcanism at Ubinas, Huaynaputina and Ticsani, southern Peru. J. Volcanol. Geotherm. Res. 186, 253–264.
Lavallée, Y., Benson, P.M., Heap, M.J., Flaws, A., Hess, K.-U., Dingwell, D.B., 2012. Volcanic conduit failure as a trigger to magmatic fragmentation. Bull. Volcanol. 74, 11–13, , http://dx.doi.org/10.1007/s00445-011-0544-2.
Lejeune, A.M., Richet, P., 1995. Rheology of crystal-bearing silicate melts—an experimental-study at high viscosities. J. Geophys. Res. 100, 4215–4229.

Lister, J.R., Kerr, R.C., 1991. Fluid-mechanical models of crack propagation and their application to magma-transport in dykes. J. Geophys. Res. 96, 10049–10077.

Massol, H., Jaupart, C., 1999. The generation of gas overpressure in volcanic eruptions. Earth Planet. Sci. Lett. 166, 57–70.

McNutt, S.R., 1996. Seismic monitoring and eruption forecasting of volcanoes; a review of the state-of-the-art and case histories. In: Scarpa, R., Tilling, R. (Eds.), Monitoring and Mitigation of Volcanic of Volcanoes. Springer, Verlag, New York, pp. 99–146.

Menand, T., Tait, S.R., 2001. A phenomenological model for precursor volcanic eruptions. Nature 411, 678–680.

Muhlbauer, M.J., Calzada, E., Schillinger, B., 2005. Development of a system for neutron radiography and tomography. Nucl. Instrum. Methods Phys. Res. A 542, 324–328.

Nakamura, K., 1977. Volcanoes as possible indicators of tectonic stress orientation—principle and proposal. J. Volcanol. Geotherm. Res. 2, 1–16.

Paterson, M.S., Wong, T.-f., 2005. Experimental Rock Deformation - the brittle field, 2nd ed. Springer, Verlag, Berlin.

Pertsov, N.V., Kogan, B.S., Balashov, V.N., 1977. Model of magma intrusions going through fractures under conditions of manifestation of effect of adsorption decrease of rock strength. Dokl. Akad. Nauk SSSR 235, 1375–1378.

Pitcher, W.S., 1979. The nature, ascent and emplacement of granitic magmas. J. Geol. Soc. London 136, 627–662.

Richter, F., 2006. Upsetting and Viscoelasticity of Vitreous SiO_2: Experiments, Interpretation and Simulation. Technischen Universität, Berlin (pp. 239).

Rocchi, V., Sammonds, P.R., Kilburn, C.R.J., 2004. Fracturing of Etnean and Vesuvian rocks at high temperatures and low pressures. J. Volcanol. Geotherm. Res. 132, 137–157.

Rubin, A.M., 1995. Propagation of magma-filled cracks. Ann. Rev. Earth Planet. Sci. 23, 287–336.

Santoni, S., Tallarico, A., Dragoni, M., 2011. Magma ascent and effusion from a tensile fracture propagating to the Earth's surface. Geophys. J. Int. 186, 681–698, , http://dx.doi.org/10.1111/j.1365-246X.2011.05060.x.

Selvadurai, A.P.S., 2000. Partial Differential Equations in Mechanics. Vol. II. The Biharmonic Equation, Poisson's Equation. Springer-Verlag, Berlin.

Selvadurai, A.P.S., Boulon, M.J. (Eds.), 1995. Developments in Applied Mechanics, vol. 42. Elsevier Science Publications, Amsterdam.

Selvadurai, A.P.S., Benson, P.M. An elastic plug test for estimating properties of Brittle Geomaterials. Int. J. Rock Mech. (in preparation).

Smith, R., Sammonds, P.R., Kilburn, C.R.J., 2009. Fracturing of volcanic systems: experimental insights into pre-eruptive conditions. Earth Planet. Sci. Lett. 280, 211–219.

Sparks, R.S.J., Bursik, M.I., Carey, S.N., Gilbert, J.S., Glaze, L.S, Sigurdsson, H., Woods, A.W., 1997. Volcanic Plumes. Wiley, New York.

Stanchits, S., Vinciguerra, S., Dresen, G., 2006. Ultrasonic velocities, acoustic emission characteristics and crack damage of basalt and granite. Pure Appl. Geophys. 163, 974–993.

Timoshenko, S.P., Goodier, J.N., 1970. Theory of Elasticity. McGraw-Hill, New York.

Tuffen, H., Dingwell, D.B., Pinkerton, H., 2003. Repeated fracture and healing of silicic magma generate flow banding and earthquakes? Geology 31, 1089–1092.

Tuffen, H., Smith, R., Sammonds, P.R., 2008. Evidence for seismogenic fracture of silicic magma. Nature 453, 511–514.

Valko, Economides, 1995. Hydraulic Fracture Mechanics. Wiley, New York.

Vinciguerra, S., Meredith, P.G., Hazzard, J., 2004. Experimental and modelling study of fluid pressure-driven fractures in Darley Dale sandstone. Geophys. Res. Lett. 31 (1–5), L09609, http://dx.doi.org/10.1029/2004GL019638.

Vinciguerra, S., Elsworth, D., Malone, S., 2005. The 1980 pressure response and flank failure of Mount St. Helens (USA) inferred from seismic scaling exponents. J. Volcanol. Geotherm. Res. 144 (2005), 155–168.

Walter, T.R., Troll, V.R., 2003. Experiments on rift zone evolution in unstable volcanic edifices. J. Volcanol. Geotherm. Res. 127, 107–120.

Xia, K., Rosakis, A.R., Kanamori, H., 2004. Laboratory earthquakes: the sub-Rayleigh-to-supershear rupture transition. Science 303, 1859–1861.